

CERN/PS/BR 76-21
1 November 1976

TRANSVERSE BUNCHED-BEAM INSTABILITIES

F.J. Sacherer

CERN, Geneva, Switzerland

Lecture to be given as Part 2 of the course on
"Single-beam collective phenomena - Transverse"
at the International School of Particle Accelerators,
Ettore Majorana Centre for Scientific Culture,
Erice, Sicily, 10-22 November 1976

TRANSVERSE BUNCHED-BEAM INSTABILITIES

F.J. Sacherer

ERRATUM

Page 13, Eq. (66) should read

$$\Delta\omega = \frac{j}{4\pi Q} \frac{c}{(\gamma E_0/e)} Z_1 I \quad (66)$$

Coupling Impedance

The purpose of this section is to show how the transverse coupling impedance Z_{\perp} can be at least roughly estimated once one has some idea of where the wall currents are and what the field lines look like.

Longitudinal

The beam sees a uniform longitudinal electric field set up by the return currents or image currents flowing in the vacuum chamber walls. For example, for resistive walls,

$$Z_{\parallel} = \frac{2\pi R}{2\pi b} \mathcal{R}_{\text{surf}} , \quad (45)$$

where $2\pi R$ = machine circumference, b = vacuum chamber radius, and $\mathcal{R}_{\text{surf}}$ is the surface impedance in ohms per square. In other words, Z_{\parallel} is the total surface resistance of a strip of length $2\pi R$ and width $2\pi b$.

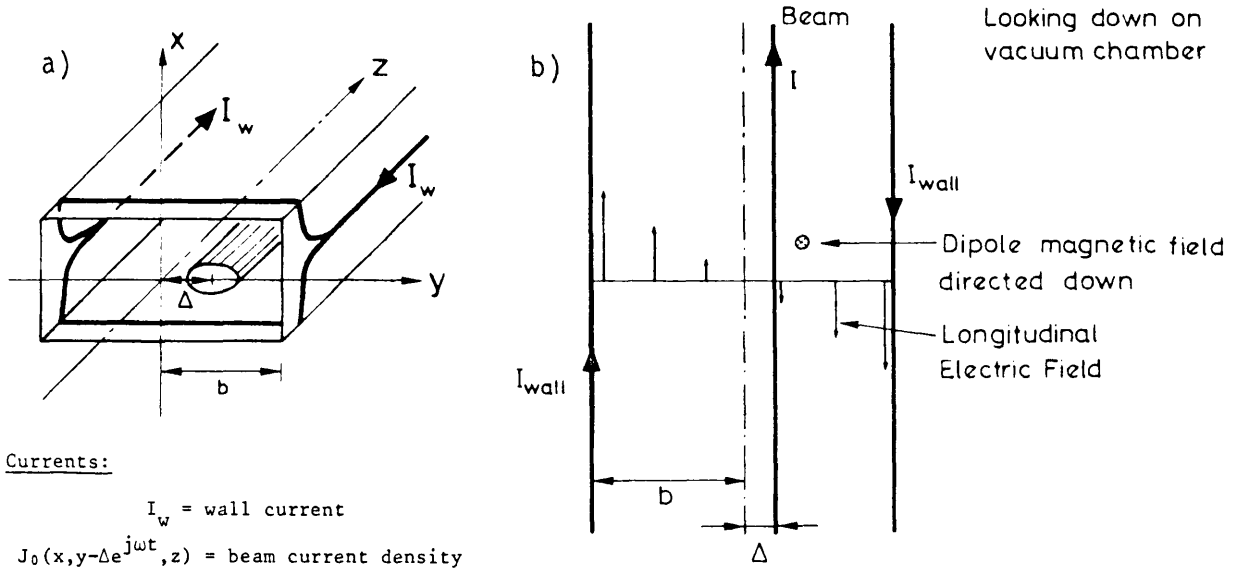
Transverse

The beam oscillates from side to side, which drives a differential wall current I_w that flows in opposite directions on either side of the vacuum chamber. This in turn requires a longitudinal electric field E_z that varies in strength across the aperture, and a transverse magnet field B_x as shown in Fig. 5. Energy extracted from the beam by the longitudinal electric field drives the wall currents, which set up the dipole magnetic field, which deflects the beam. The wall currents can be found by equating the power lost per unit length by the beam due to the E_z field,

$$\int \mathbf{E} \cdot \mathbf{J} \, dx \, dy = - \frac{E_0 \Delta}{b} \int y \frac{\partial J_0}{\partial y} \, dx \, dy = \frac{E_0 \Delta}{b} I \quad (46)$$

to the power flow into the walls, $-2I_w E_0$, namely

$$I_w = - \frac{1}{2} \frac{\Delta}{b} I . \quad (47)$$



Currents:

I_w = wall current
 $J_0(x, y - \Delta e^{j\omega t}, z)$ = beam current density
 $\approx J_0(x, y, z) - \frac{\partial J_0}{\partial y} \Delta e^{j\omega t}$

with

I = beam current = $\int J_0(x, y, z) dx dy$.

Fields:

$E_z = E_0 \frac{y}{b} e^{j\omega t}$ (median plane)

$B_x = \frac{j}{\omega} \frac{E_0}{b} e^{j\omega t}$ (from $\nabla \times E + \dot{B} = 0$).

Fig. 5

This current is related to the electric field at the wall E_0 by the wall impedance $Z_{||}$. Assume that I_w is concentrated in a strip of width of about $\frac{1}{4}$ the pipe circumference on either side of the beam, as shown in Fig. 5. Then the effective impedance is $4Z_{||}$ and

$$V = 4I_w Z_{||} = 2\pi R E_0 ,$$

or

$$E_0 = 4 \frac{I_w Z_{||}}{2\pi R} . \tag{48}$$

This gives the correct result for a round pipe, which has a $\cos \theta$ current distribution. The deflecting magnetic field is (from Fig. 5)

$$B_x = -j \frac{2\Delta}{\omega b^2} \frac{Z_{||} I}{2\pi R} e^{j\omega t} , \tag{49}$$

and when this is inserted into the definition of Z_{\perp} ,

$$Z_{\perp} = j \frac{2\pi R \int_0^{\Delta} [E + v \times B]_{\perp} ds}{\beta I \Delta} , \quad (\text{ohms/metre}), \tag{50}$$

one finds

$$Z_{\perp} = \frac{2c}{b^2} \frac{Z_{\parallel}}{\omega}, \quad (51)$$

where c is the speed of light (3×10^8 m/sec) and $\beta = v/c$. This convenient relation between $Z_{\perp}(\omega)$ and $Z_{\parallel}(\omega)$ is strictly valid for a round pipe with surface impedance $\mathcal{R}_{\text{surf}}$ and for frequencies sufficiently below cut-off that the fields have the simple form shown in Fig. 5. On the other hand, for perfectly conducting walls ($\mathcal{R}_{\text{surf}} = 0$), Z_{\perp} is capacitive,

$$Z_{\perp} = -j \frac{RZ_0}{\beta^2 \gamma^2} \left(\frac{1}{a^2} - \frac{1}{b^2} \right), \quad (52)$$

where $Z_0 = 377$ ohms, a = beam radius, and b = pipe radius. The additional contribution due to wall resistivity can be found from (45) and (51) with

$$\mathcal{R}_{\text{surf}} = (1 + j) \frac{\rho}{\delta} \quad (\text{thick-wall}), \quad (53)$$

where ρ is the resistivity (ohm-m) and δ is the skin depth. At sufficiently low frequencies, $\delta >$ wall thickness l , and we should use

$$\mathcal{R}_{\text{surf}} = \frac{\rho}{l} \quad (\text{thin-wall}) \quad (54)$$

provided the impedance of any alternate current paths outside the vacuum chamber is sufficiently high that all currents flow through the walls. Since $\delta \propto \omega^{-1/2}$, Z_{\perp} has the form shown in Fig. 6.

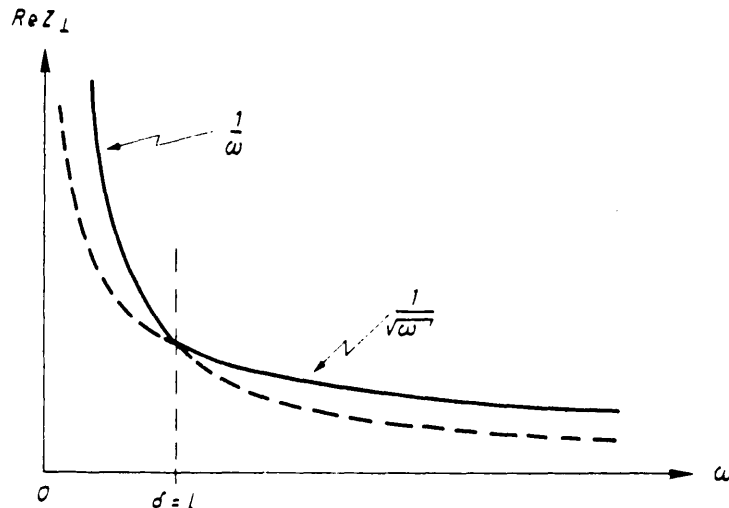


Fig. 6 Real part of resistive-wall impedance

A simple case where Eq. (51) does not work is shown in Fig. 7, namely a high impedance interruption in the vacuum chamber, for example a ceramic tube with a resistive coating. The longitudinal impedance $Z_{||}$ is increased, but not the transverse since the differential currents can avoid the high impedance region as shown. The transverse impedance is increased only at very high frequencies where the wavelength becomes comparable to the interruption length or pipe circumference, or in other words, where the added inductance due to the more circuitous path begins to contribute. Roughly speaking, this occurs around the pipe cut-off frequency, typically between 1 and 2 GHz.

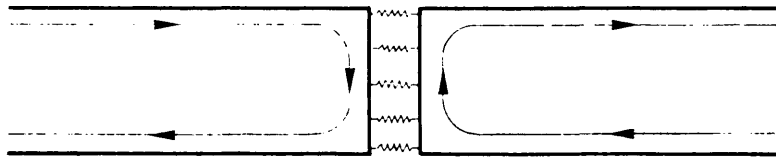


Fig. 7 Interruption in vacuum chamber

Figure 8 shows an actual measurement of the resistive part of the impedance for the PS over a frequency range up to 2 GHz. An effective $Z_{||}/n$ computed from Eq. (51) is plotted instead of the less familiar Z_{\perp} . The measurement technique⁶⁾ uses the beam and will be described later. The actual impedance is much larger than the resistive-wall value, which is not too surprising considering the large number of interruptions in the vacuum chamber for PU electrodes, septum tanks, ferrite kicker magnets, bellows, vacuum manifolds, etc.

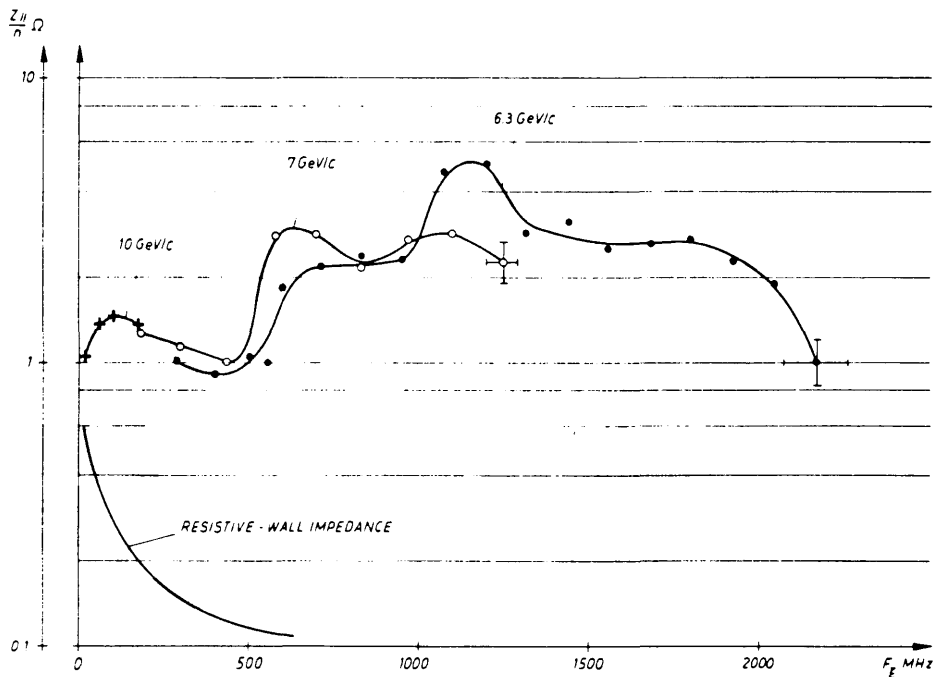


Fig. 8 Measured impedance of the PS⁶⁾


In short, any structure that supports a longitudinal electric field that varies across the aperture, or equivalently allows wall current loops that produce a dipole magnetic field, will increase Z_{\perp} .

Modes of Oscillation

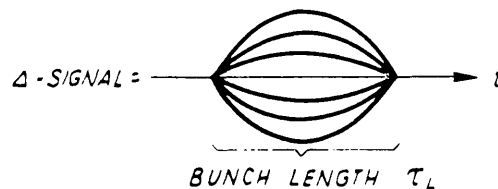
Zero chromaticity

$$\xi = \frac{dQ}{Q} / \frac{dp}{p} = 0 ,$$

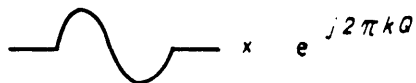
so all particles have the same betatron frequency Q . The bunch can oscillate up and down as a rigid unit, the so-called rigid-bunch mode ($m = 0$). The signal on a position monitor has the form

$$\Delta\text{-signal} \propto p_0(t) e^{j2\pi k Q} = \text{---} \text{---} \text{---} \times e^{j2\pi k Q}$$


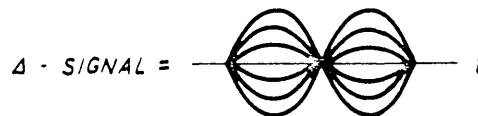
on the k^{th} revolution, or summed over many revolutions,



For the $m = 1$ mode, the front of the bunch moves up while the back moves down, with the centre stationary,

$$\Delta\text{-signal} \propto p_1(t) e^{j2\pi k Q} = \text{---} \text{---} \text{---} \times e^{j2\pi k Q}$$


or summed over several revolutions



In the synchrotron phase space of Fig. 9, the particles are arranged around the synchrotron orbit so that their transverse dipole moment p is up near the front of the bunch and down near the back, as shown. After half a betatron oscillation, the signs are reversed. On a slower time-scale, the oscillating dipoles are carried around the synchrotron orbit, but note that the net dipole moment near the bunch centre $\theta = 0$ is always zero owing to cancellation between $+\Delta p/p$ and $-\Delta p/p$ particles. If ϕ is the synchrotron phase along an orbit, the mode patterns are described by $e^{jm\phi}$.

above or below a $\frac{1}{2}$ integer, and on the sign of the wake field. For resistive-wall wakes, single-bunch instability occurs for Q-values above a $\frac{1}{2}$ integer.

If many bunches are present, coupled motion of the different bunches is possible with one bunch driving the next, and so on. For M bunches, M coupled-bunch modes are possible, with a phase shift of $2\pi n/M$ between bunches for coupled-bunch mode n, as shown in Fig. 10. Now, about half the modes are unstable for any choice of Q-value.

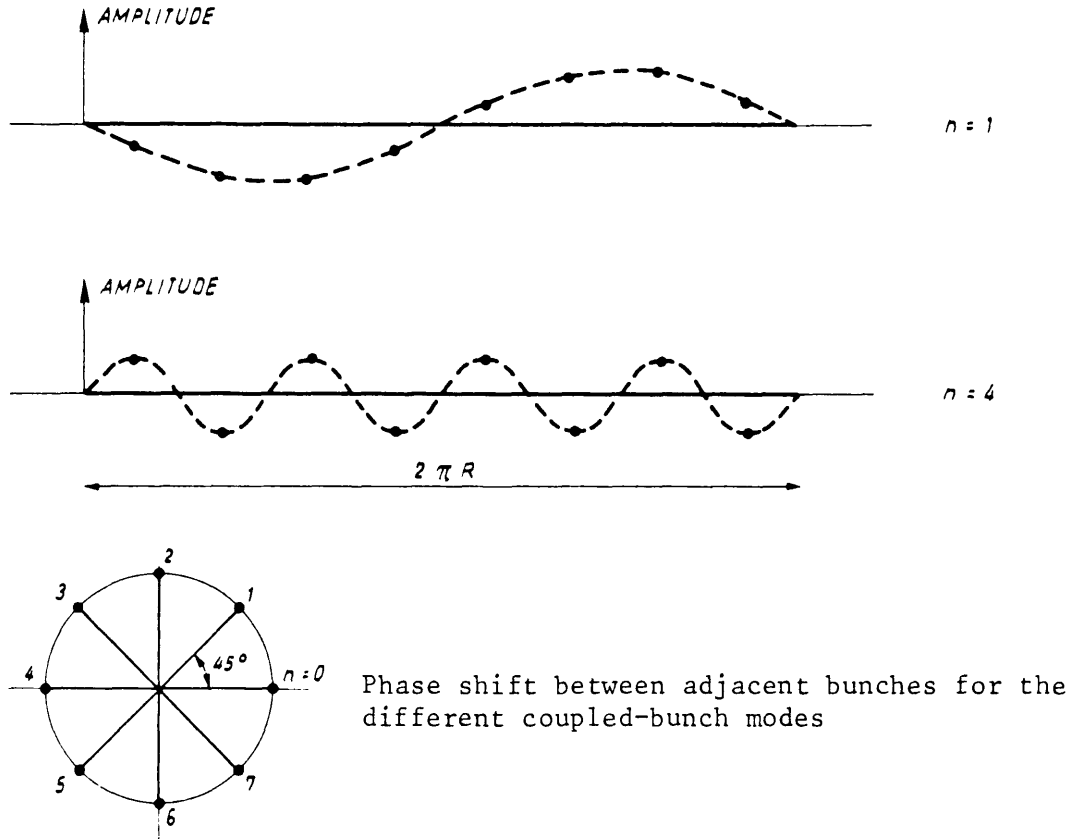
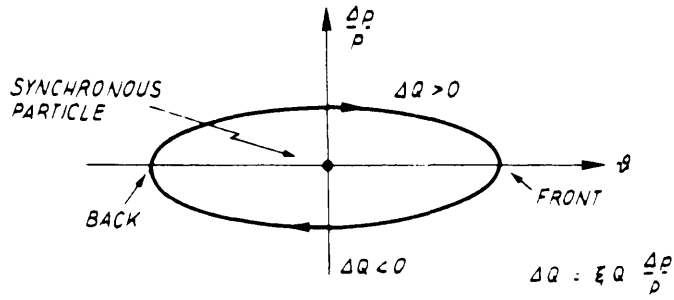


Fig. 10 Coupled-bunch modes for eight bunches

Non-zero chromaticity

With finite chromaticity, the betatron frequency Q varies around a synchrotron orbit. Assume the chromaticity ξ is positive, and that we are below transition energy so that the particles move clockwise around the synchrotron orbit as shown in the following diagram. A particle at the front of the bunch has the same betatron frequency as the synchronous particle, and we assume it has the same phase also. As the particle moves back along the synchrotron orbit, its phase gradually slips behind that of the synchronous particle ($\Delta Q < 0$) until it reaches the back of the bunch. Then as it moves forward again ($\Delta Q > 0$), its phase advances and returns to the starting value when the particle regains the front of the bunch. The phase along the bunch is indicated schematically



in Fig. 11 by the length of the arrows (down for phase lag) rather than the plus or minus signs of the previous drawings.

If we now place particles around the orbit and arrange their betatron phase initially to be as indicated in Fig. 11, the pattern remains stationary, and the given phase relationship along the bunch is preserved in time. For example, as a particle leaves the back of the bunch, another always arrives with the correct accumulated phase shift to replace it. Thus the front and back of the bunch oscillate with a phase difference, which reduces to rigid-bunch oscillation only in the limit of zero chromaticity.

The total phase shift between head and tail is usually denoted by χ . It can be computed as follows. The betatron frequency depends on the momentum deviation

$$\Delta Q = \xi Q \frac{\Delta p}{p}, \quad (55)$$

which in turn is related to the deviation in revolution times,

$$\frac{\Delta p}{p} = \frac{1}{\eta} \frac{\Delta T}{T}, \quad (56)$$

where T is the revolution period, $\eta = 1/\gamma_T^2 - 1/\gamma^2$, and gamma transition γ_T is usually about $\gamma_T \approx Q_H$. We can specify the location of the particle within

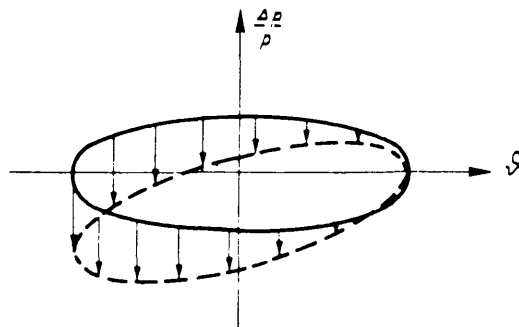


Fig. 11 Betatron phase around a synchronous orbit

the bunch by giving its time delay τ from the head of the bunch. This time delay changes by the amount ΔT per revolution, or

$$\frac{d\tau}{dk} = \Delta T .$$

The accumulated betatron phase shift is

$$\begin{aligned} \chi &= 2\pi \int \Delta Q \, dk \\ &= \frac{2\pi}{T} \frac{\xi}{\eta} Q \int \frac{d\tau}{dk} \, dk \\ &= \frac{\xi}{\eta} Q \omega_0 \tau , \end{aligned} \tag{57}$$

where $\omega_0 = 2\pi/T$. Thus the phase varies linearly along the bunch and attains its maximum value at the tail where $\tau =$ bunch length τ_L .

In terms of the bunching factor $B =$ bunch length/bunch separation and the number of bunches M ,

$$\chi = \frac{\xi}{\eta} \frac{2\pi Q}{M} B . \tag{58}$$

This is plotted as a function of energy or γ in Fig. 12 for the "natural" machine chromaticity $\xi = -1$. In general, χ can be several radians, and approaches infinity at transition energy.

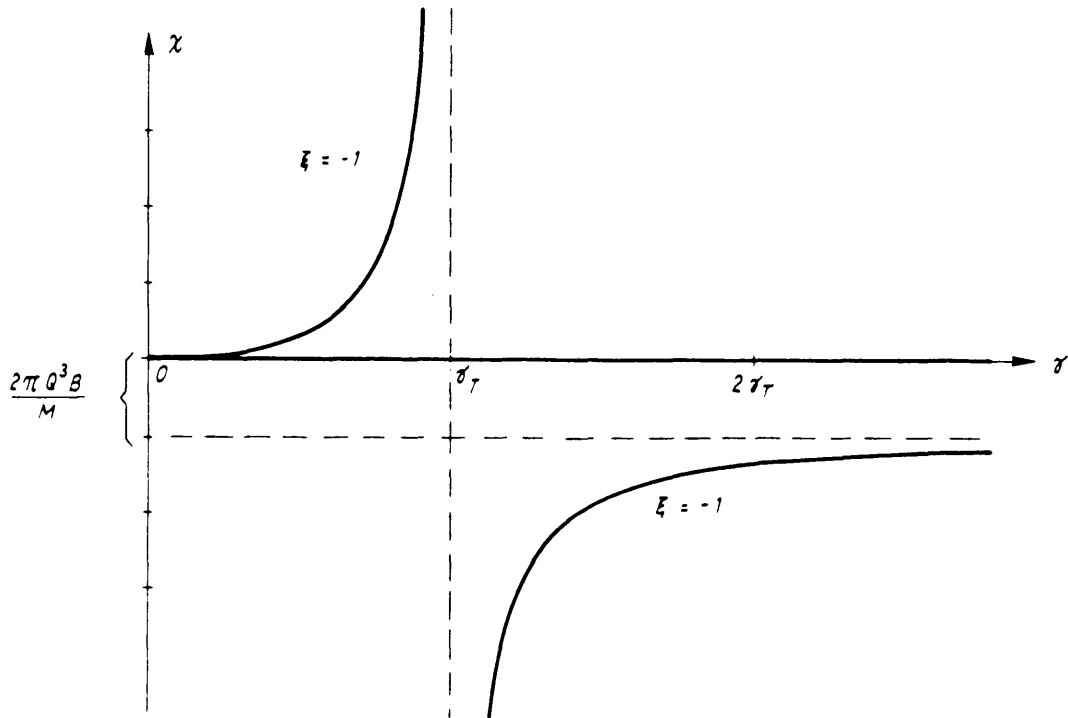


Fig. 12 Head-tail phase shift χ versus energy

The same linear phase-shift along the bunch occurs for the higher modes $m \neq 0$, but the amplitude of oscillation is given by the standing-wave pattern $p_m(t)$. The PU signal has the form (Fig. 13)

$$\Delta\text{-signal} \propto p_m(t) e^{j\omega_\xi t + j2\pi kQ}, \quad (59)$$

where

$$\omega_\xi = \frac{\chi}{\tau_L} = \frac{\xi}{\eta} Q\omega_0$$

gives the frequency (radians/sec) of the wiggles along the bunch ($f_\xi = \omega_\xi/2\pi$ in Hz). The number of nodes still determine the head-tail mode number m .

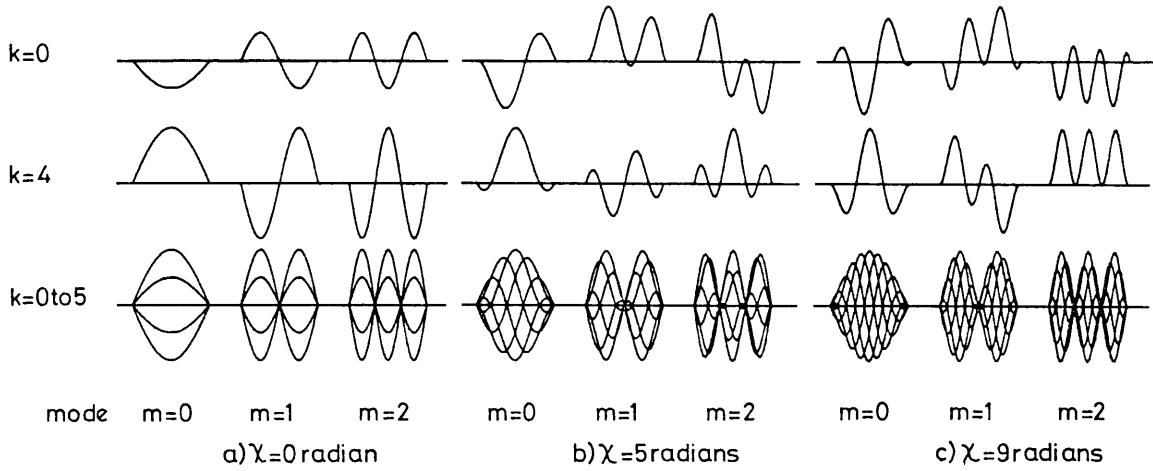


Fig. 13 Δ -signal of a single bunch on separate revolutions, and with six revolutions superimposed. Vertical axis is difference signal from position monitor, horizontal axis is time, and $Q = 4.833$.

Figure 14 shows some head-tail modes observed in the PS Booster⁶⁾ for different values of χ .

Frequency domain

The Fourier transform of the signals (59) gives the frequency components. The standing-wave patterns $p_m(t)$ can be taken to be sinusoidal,

$$p_m(t) = \begin{cases} \cos (m+1)\pi \frac{t}{\tau_L} & m = 0, 2, 4, \dots \\ \sin (m+1)\pi \frac{t}{\tau_L} & m = 1, 3, 5, \dots \end{cases} \quad (60)$$

The Fourier transform is $\tilde{p}_m(\omega)$, and for the "power spectrum" $h_m(\omega) = |\tilde{p}_m(\omega)|^2$, we find

$$h_m(\omega) = (m+1)^2 \frac{\tau_L^2}{2\pi^4} \frac{1 \pm \cos \pi y}{[y^2 - (m+1)^2]^2}, \quad (61)$$

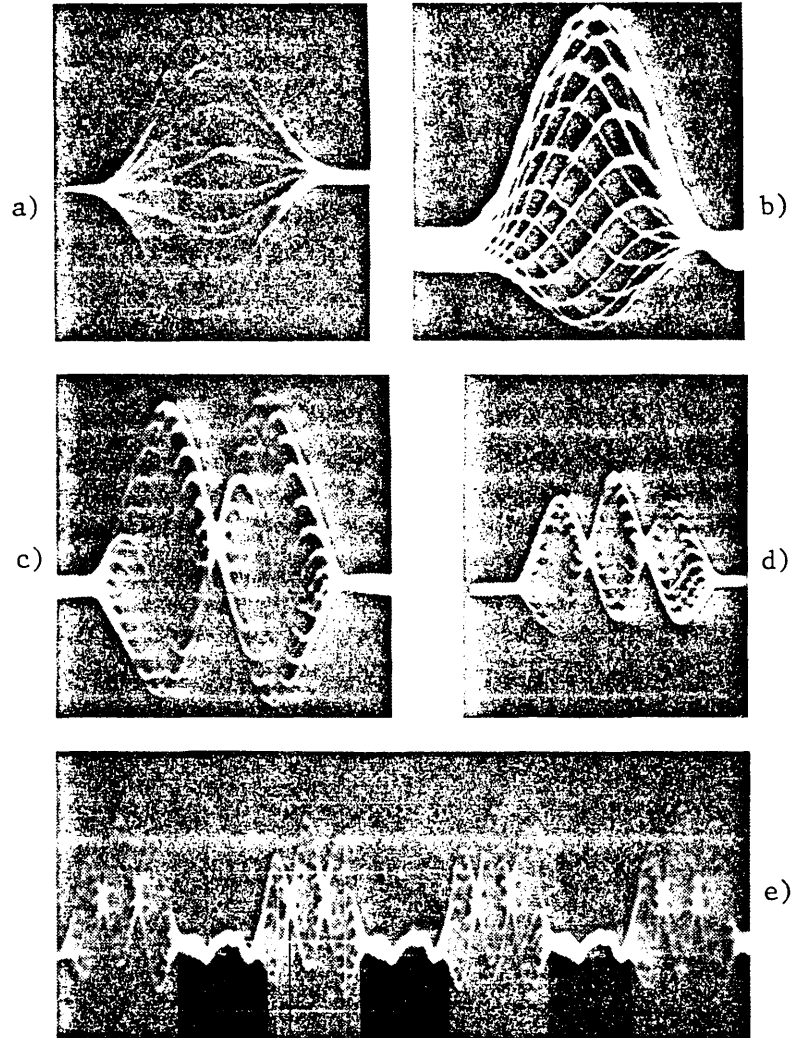


Fig. 14 A single bunch seen on about 20 consecutive revolutions. Vertical axis: Δ PU signal. Horizontal axis: time (50 nsec div.).
 a-b-c-d: with wide-band PU (bandwidth \approx 150 MHz)
 e : with normal PU (bandwidth \approx 40 MHz, and baseline restitution circuit acting).

where $y = \omega\tau_L/\pi$ and the plus sign occurs for m even, the minus sign for m odd. The different spectra are drawn in Fig. 15 for both positive and negative frequency components. The spectrum for mode zero falls off at about $f = 1/\tau_L$, as one would expect. The higher modes are sine waves with a duration of τ_L seconds so the spectra have widths of about $1/\tau_L$ Hz and are centred on the frequency of the sine wave, namely $(m+1)/2\tau_L$ for mode m . This mode has m nodes, and therefore $m + 1$ half wavelengths or $(m+1)/2$ full wavelengths in a time of τ_L seconds.

The spectrum is symmetric because $p_m(t)$ is a standing wave, i.e.

$$\cos \omega t = \frac{1}{2}(e^{j\omega t} + e^{-j\omega t}) .$$

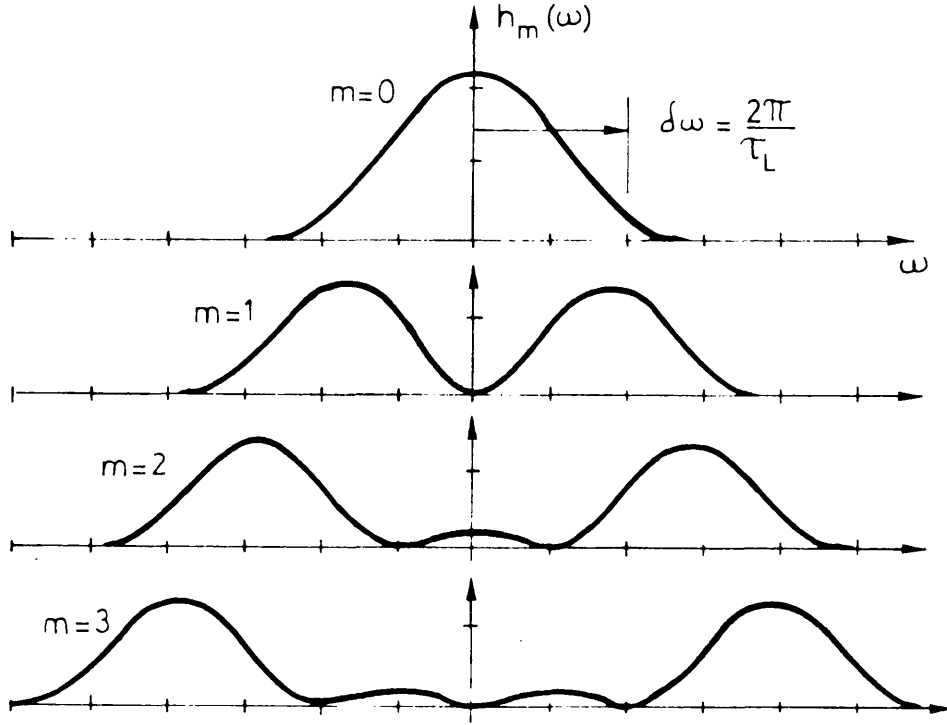


Fig. 15 Frequency spectrum for modes 0 to 3 with $\chi = 0$

For finite chromaticity, the travelling-wave component $e^{j\omega_\xi t}$ is also present, and the spectrum is shifted,

$$h_m = h_m(\omega - \omega_\xi) ,$$

toward positive or negative frequencies depending on the sign of ω_ξ . This is easy to see with a spectrum analyser.

The actual spectrum is a line spectrum within the envelope $h_m(\omega - \omega_\xi)$. For a single bunch, the frequencies

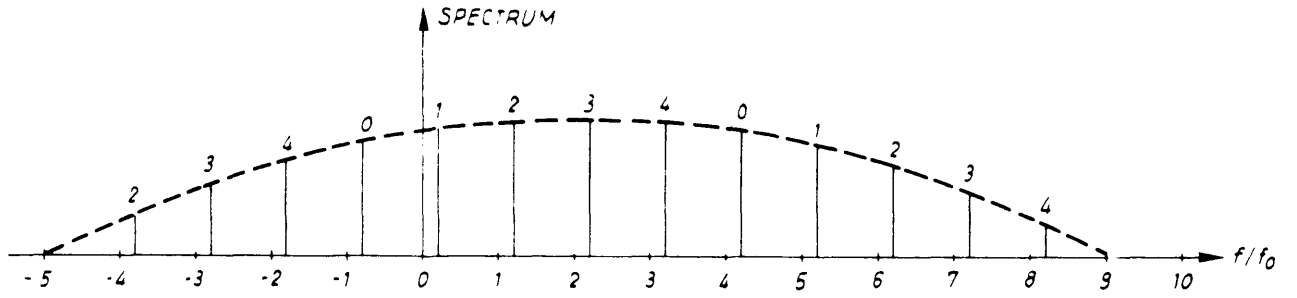
$$\omega_p = (p + Q)\omega_0 , \quad -\infty < p < \infty , \quad (62)$$

occur where p is any integer positive or negative. For M equally spaced bunches, only every M^{th} line occurs. For coupled-bunch mode n , the frequencies are

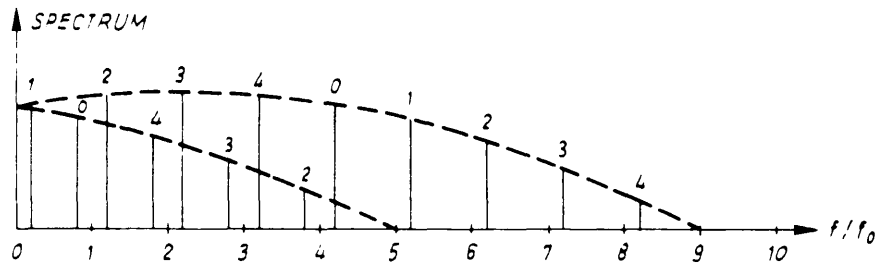
$$\omega_p = (p + Q)\omega_0 , \quad p = n + kM , \quad (63)$$

where k is any integer positive or negative, and the mode number n is positive or zero. A typical spectrum for a machine with five long bunches (PS Booster) and $Q = 4.2$ is shown in Fig. 16 for the different possible coupled-bunch modes n . The envelope is drawn for head-tail mode $m = 0$ and is shifted towards positive frequencies ($f_\xi \approx 2f_0$). For shorter bunches, the spectrum would extend much further in frequency.

We can now recognize the different head-tail modes in either time or frequency domain.



a) with positive and negative frequencies



b) as seen by a spectrum analyser

Fig. 16

Growth Rates

First consider a coasting beam. The equation of motion for a single particle

$$\ddot{x} + Q^2 \omega_0^2 x = -j \frac{e\beta}{\gamma m_0} \frac{Z_{\perp} I}{2\pi R} x \quad (64)$$

follows immediately from the definition (50) of Z_{\perp} . The RHS of (64) causes the frequency shift

$$\begin{aligned} \Delta\omega &= \frac{j}{2Q\omega_0} \frac{e\beta}{\gamma m_0} \frac{Z_{\perp} I}{2\pi R} \quad (\text{coasting beam}) \\ &= U + (1-j)V \end{aligned} \quad (65)$$

and growth-rate

$$\frac{1}{\tau} = -\text{Im } \Delta\omega ,$$

where the time dependence $e^{j\omega t}$ has been assumed^{*)}. The impedance Z_{\perp} is evaluated at the frequency $\omega = (p + Q)\omega_0 + \Delta\omega$ for the mode with $|p|$ wavelengths around the machine circumference $2\pi R$. Here $\beta = v/c$ and I is the d.c. current. Equation (65) can also be written as

$$\Delta\omega = \frac{j}{4\pi} \frac{c}{(E_0/e)} Z_{\perp} I , \quad (66)$$

*) To compare with papers using $e^{-i\omega t}$, replace j with $-i$ in all formulae.

where $E_0/e = 0.938 \times 10^9$ V for protons (0.511×10^6 V for electrons),
 $c = 3 \times 10^8$ m/sec, Z_{\perp} in ohms/m and I in amperes.

Note that the reactive part of $Z_{\perp}(\omega)$ produces a real frequency shift $\Delta\omega$ while the resistive part $\text{Re } Z_{\perp}(\omega)$ causes instability for negative resistance and damping for positive resistance. Negative resistance occurs for negative frequencies [see Eq. (51)], and therefore only coasting-beam modes with $p < -Q$ can be unstable.

For the bunched beam, the growth-rate involves a sum over the bunch spectrum. In fact, the power spectrum $h_m(\omega) = |\tilde{p}_m(\omega)|^2$ enters because $Z_{\perp}(\omega)\tilde{p}_m(\omega)$ gives the deflecting field, which must be integrated over the bunch to get the total force, so

$$\Delta\omega_m \propto \sum Z_{\perp}(\omega) |\tilde{p}_m(\omega)|^2 .$$

The final result can be written as

$$\Delta\omega_m = \frac{1}{1+m} \frac{j}{2Q\omega_0} \frac{e\beta}{\gamma m_0} \frac{I_0}{L} \frac{\sum Z_{\perp}(\omega) h_m(\omega - \omega_{\xi})}{\sum h_m(\omega - \omega_{\xi})} , \quad (67)$$

where the summations are over the mode spectra (62) for a single bunch, or (63) for M bunches. This expression is very similar to the coasting-beam formula (65) except that $I/2\pi R$ is replaced by the current in one bunch $I_0 = I/M$ divided by the bunch length L (metres). The factor $(1+m)^{-1}$ in front indicates that the higher modes are more difficult to drive.

Equation (67) is the general result. In the limit of short-range wakes or broadband $Z_{\perp}(\omega)$, it reduces to the classic head-tail effect, while in the opposite limit of long-range or narrowband $Z_{\perp}(\omega)$, it reduces to the multiturn or coupled-bunch type of instability.

Figure 17 shows an example with broadband $Z_{\perp}(\omega)$. The spectrum is drawn for head-tail mode $m = 0$ with positive phase-shift χ , so we are above transition with $\xi > 0$ or below transition with $\xi < 0$. The phase shift $\chi = 3 \times 2\pi$ radians corresponds to three oscillations along the bunch. The resistive part of $Z_{\perp}(\omega)$ is drawn in for a resistive-wall type impedance. Clearly mode $m = 0$ is stable in this case. In fact, as long as the discrete nature of the spectrum can be ignored, mode $m = 0$ is stable for χ positive and unstable for χ negative for any type of impedance. However, if the spectrum overlaps the narrowband region of $Z_{\perp}(\omega)$ near zero frequency, an individual spectrum line can dominate, especially one very near zero frequency.

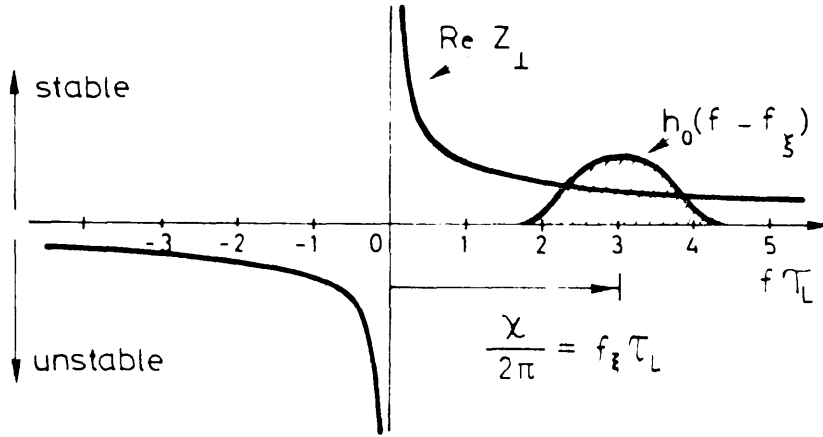


Fig. 17

For Fig. 17, $Z_{\perp}(\omega)$ is sufficiently smooth that it can be removed from the summation in Eq. (67), and we find

$$\Delta\omega_0 = \frac{j}{2Q\omega_0} \frac{e\beta}{\gamma m_0} \frac{Z_{\perp}(\omega_{\xi})I}{2\pi RB}, \quad (68)$$

which is just the coasting-beam result (65) for the frequency ω_{ξ} with a bunching factor included ($B = ML/2\pi R$, $I = MI_0$). If ω_{ξ} can be varied, by changing the chromaticity for example, the impedance $\text{Re } Z_{\perp}(\omega_{\xi})$ can be deduced by measuring the growth-rate, $\text{Im } \Delta\omega_0$. This is how the impedance Fig. 8 of the PS was measured⁶⁾. For the PS, the spectrum $h_0(\omega)$ has a width of $\sim \pm 100$ MHz and f_{ξ} can be varied from zero to ~ 2 GHz by working on a magnetic flat-top near transition energy. Fortunately, only mode $m = 0$ grows, so the measurements are easy to interpret.

In the opposite limit of a narrowband impedance, where only a single frequency ω_n contributes to the summation in Eq. (67),

$$\Delta\omega_m = \frac{1}{1+m} \frac{j}{2Q\omega_0} \frac{e\beta}{\gamma m_0} \frac{IZ_{\perp}}{2\pi R} F'_m(\chi - \omega_n \tau_L), \quad (69)$$

where the form factor

$$F'_m = \frac{1}{B} \frac{h_m(\omega_{\xi})}{\sum h_m(\omega)}$$

is plotted in Fig. 18. This is again the coasting-beam result (65), but reduced by the factors F'_m and $(1+m)^{-1}$. Figure 19 shows an example. For independent bunch motion, multiply (69) by $1/M$.

A less obvious case is the resistive-wall impedance shown in Fig. 20, but here also only a single line contributes to the long-range part of the wake, namely the line $\omega_n = (n+Q)\omega_0$ nearest the origin, in the narrowband

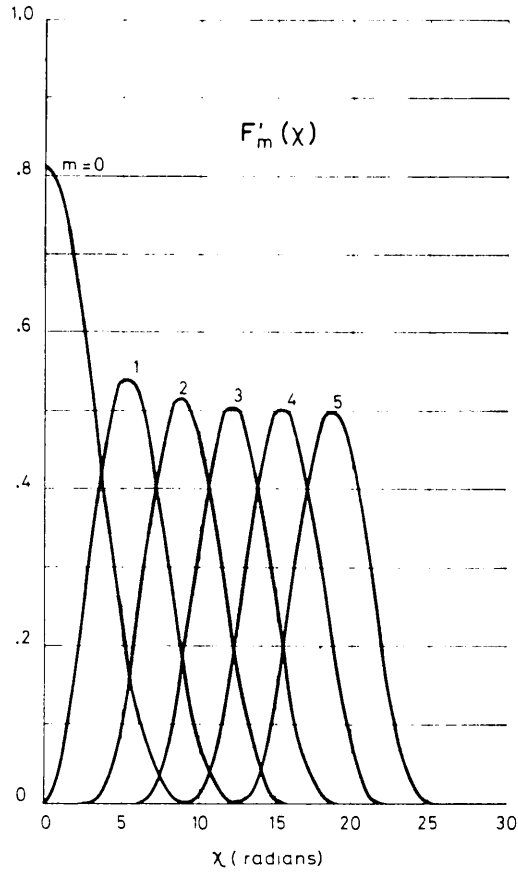


Fig. 18

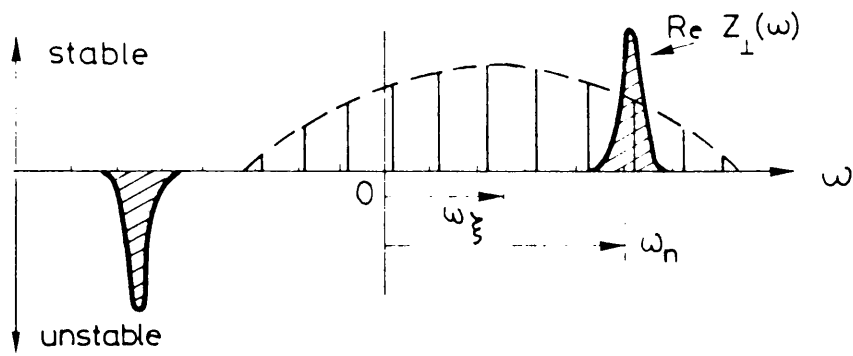


Fig. 19

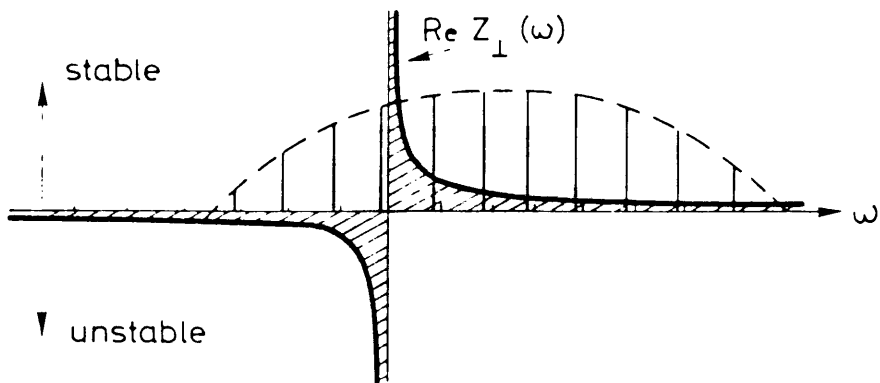


Fig. 20 The frequencies $\omega_n = (n + Q)\omega_0$ drawn for mode $m = 0$ and Q just below an integer

region of Z_{\perp} . This contribution is destabilizing for Q -values just below an integer n , and stabilizing above. In the limit $\xi = 0$ and for the thick-wall impedance (53), the multiturn effect (69) reduces to the usual Courant and Sessler rigid-bunch formula⁷⁾. However, ξ is rarely zero, and often the frequency $|n - Q|f_0$ is sufficiently small that the thin-wall impedance (54) applies with consequently larger growth-rates. This occurs for the PS Booster⁶⁾. In this case, head-tail modes 1 and 2 are driven by the long-range part of the resistive-wall wake (see Fig. 21). The photos in Fig. 14 show how the instability can be shifted from mode to mode by varying the chromaticity, and Fig. 22 shows the strong dependence of growth-rate on Q -value for Q -values just below an integer. The results agree with the thin-wall impedance expected for low frequencies $|n - Q|f_0$.

Now consider only the near-field part of $Z_{\perp}(\omega)$. This is equivalent to replacing the discrete line spectrum by a continuous spectrum. As an example, the growth-rates of modes 0 and 2 for a resistive-wall impedance are sketched

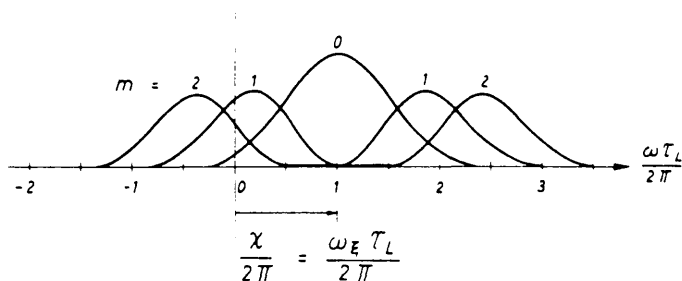


Fig. 21 Frequency spectrum for modes 0, 1, and 2 drawn for $\chi = 2\pi$

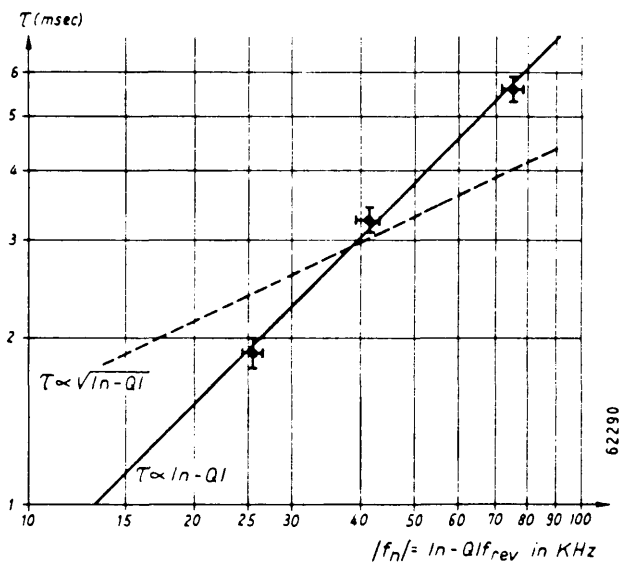


Fig. 22 e-folding time versus Q on 70 MeV flat top normalized to $I = 100$ mA

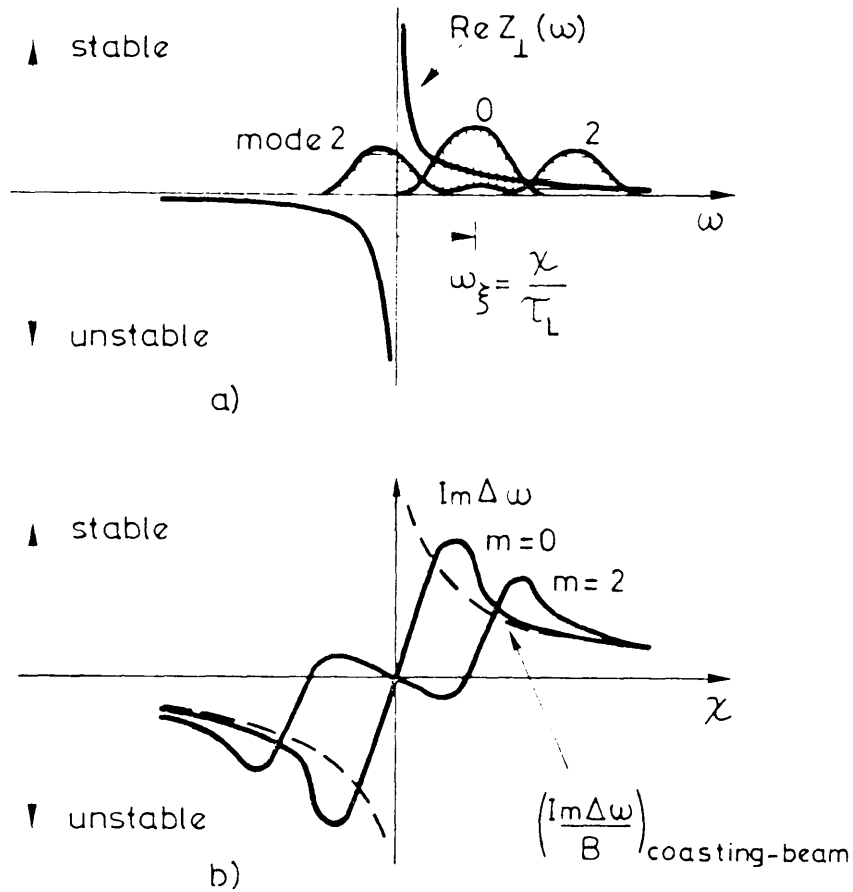


Fig. 23

in Fig. 23. As pointed out above, mode 0 is stable for positive χ , but it can be seen that mode 2 is unstable for small positive χ , and the reason is evident from Fig. 23a. For χ sufficiently large, both modes have the same stability character as the coasting beam. The exact result for the thick-wall impedance (53) and sinusoidal modes is shown in Fig. 24, and the growth-rate is found from

$$\Delta\omega_m = \frac{j}{1+m} \frac{e\beta I}{2Q\omega_0 \gamma m_0 2\pi R} \times \left[\sqrt{\frac{\pi}{MB}} |Z_{\perp}(\omega_0)| F_m(\chi) + Z_{\perp}(\omega_n) F'_m(\chi - \omega_n \tau_L) \right]. \quad (70)$$

On the other hand, for more realistic-type impedances such as that measured in the PS (Fig. 8), the higher-order head-tail modes may be stable for χ positive. From Fig. 25 it can be seen that in this case the broad positive part of the spectrum contributes more than the narrow region of negative frequencies near the origin.

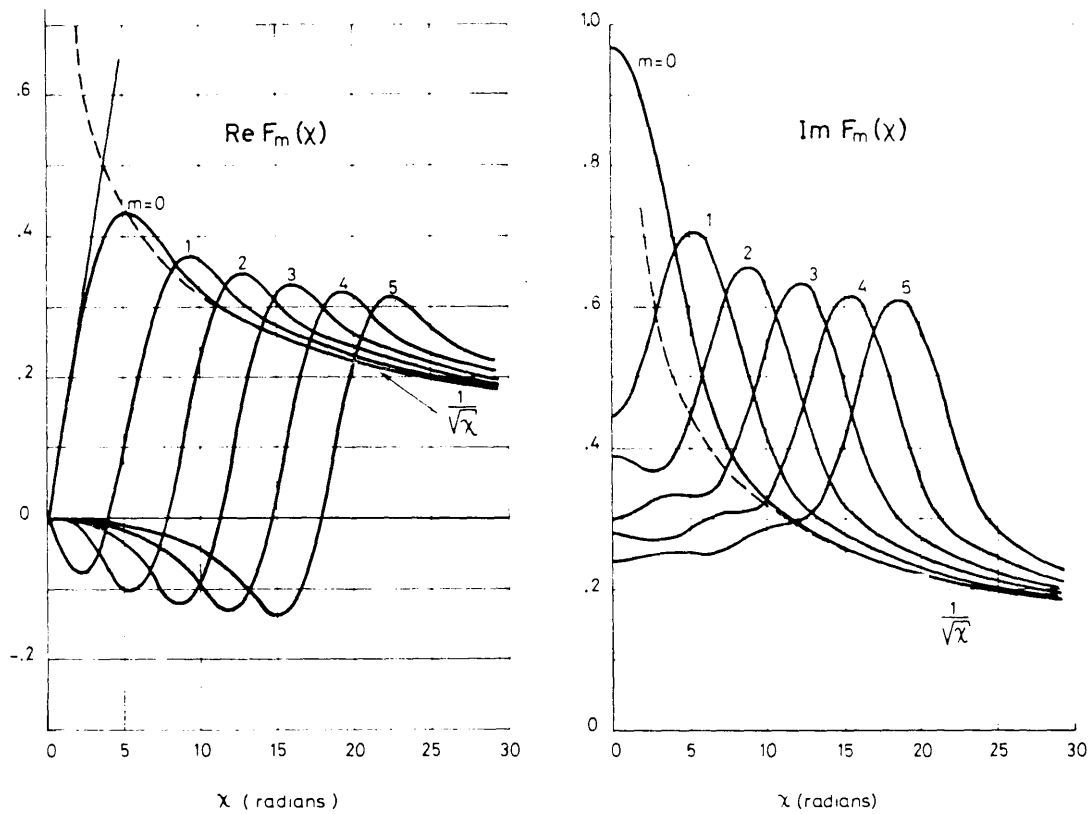


Fig. 24

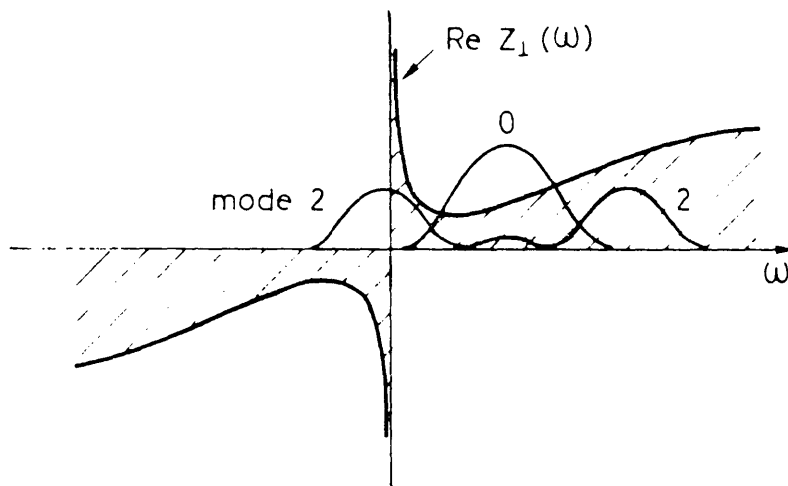


Fig. 25

Stabilization

A sufficient spread in bunch frequencies prevents the coupled-bunch type of instability. A rule-of-thumb criterion for decoupled motion is that the r.m.s. spread in bunch frequencies should exceed the growth-rate. The spread may arise from a difference in bunch populations via the coherent Laslette Q-shift.

Octupoles cure either single-bunch or coupled-bunch instability if they produce enough frequency spread within a bunch to prevent its coherent motion, that is provided the spread in betatron frequencies exceeds the frequency shift $\Delta\omega_m$,

$$|\text{full-spread at half-height of } Q\omega_0| > |\Delta\omega_m|. \quad (71)$$

Sextupoles or changes in machine chromaticity change the phase-shift χ , but do not contribute to Landau damping. For the long-range resistive-wall instability observed in the PS Booster, increasing χ shifts the instability to higher-order modes which have slower growth-rates. The opposite occurs for the PS or electron storage rings, namely the growth-rate increases as χ is made more negative.

An electronic feedback system can also be used (Fig. 26). Its action on the beam can be described in terms of an effective impedance Z , which depends on the distance between pick-up and deflector, and the electronic gain and time delays. The effect on a given mode can be seen from Eq. (65) for coasting beams or Eq. (67) for bunched beams.

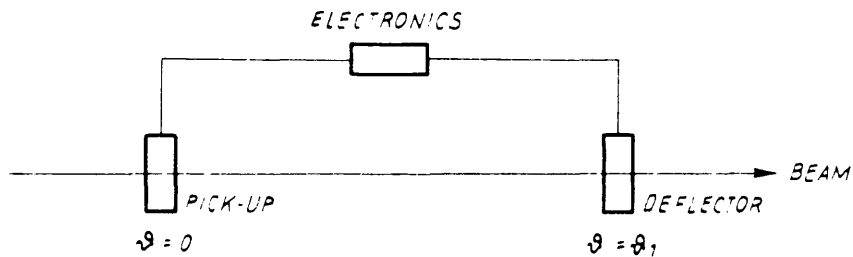


Fig. 26

Historical note

The original work on transverse bunched-beam instability was done by Courant and Sessler⁷⁾, who treated a rigid bunch driven by resistive-wall wake fields. A few years later, Pellegrini⁸⁾ and Sands⁹⁾ pointed out the very important effect of finite chromaticity, which results in non-rigid bunch oscillation. Most of the material for this lecture was drawn from Ref. 10, which combined and extended the two previous theories. At the present time, the theory appears to be in reasonably good shape in the sense that given any transverse coupling impedance, its effect on the beam can be quickly computed. What are missing are measurements and calculations of $Z_{\perp}(\omega)$.

REFERENCES

- 6) J. Gareyte and F. Sacherer, Head-tail type instabilities in the PS and Booster, Proc. 9th Internat. Conf. on High-Energy Accelerators, Stanford, 1974 (CONF 740522, US Atomic Energy Commission, Washington, D.C., 1974), p. 341.
- 7) E.D. Courant and A.M. Sessler, Rev. Sci. Instrum. 37, 1579 (1966).
- 8) C. Pellegrini, Nuovo Cimento 64A, 477 (1969).
- 9) M. Sands, SLAC-TN-69/8 and 69/10.
- 10) F. Sacherer, Transverse bunched-beam instability -- theory, Proc. 9th Internat. Conf. on High-Energy Accelerators, Stanford, 1974 (CONF 740522, US Atomic Energy Commission, Washington, D.C., 1974), p. 347.